International Journal of Applied Engineering Research ISSN 0973-4562 Volume 17, Number 5 (2022) pp. 486-499
 https://dx.doi.org/10.37622/IJAER/17.5.2022.486-499

Three-Dimensional Williamson MHD Fluid Embedded with Indium Nitride Nanoparticles Over a Linearly Stretching Porous Sheet with Radiation and Arrhenius Activation Energy

M. Jyotshna* and V. Dhanalaxmi

Department of Mathematics, University College of Technology, Osmania University. Hyderabad, 500007, India.

**Department of Mathematics, Maturi Venkata Subba Rao Engineering College (Affiliated to Osmania University) Nadergul, Hyderabad – 501510, India.*

Abstract

Several new approaches in the study of thermophysical properties have spurred various interesting dimensions in understanding the flow and heat transfer effects in nanofluids which led to new applications. Studies on nanofluids consisting of various metal, ceramic and magnetic nanoparticles added with base fluids like water, Kerosene, and Ethylene Glycol were made. But, studies with semiconductor nanoparticles are limited. Indium Nitride, a binary semiconductor, having a good amount of heat convection mixed with base fluid water in its nanoparticle form is used for the study. Three-dimensional Williamson MHD nanofluid (InN nanoparticles + water) is studied over a stretching sheet consisting of porosity under the influence of convective boundary conditions, thermal radiation, and activation energy. Using similarity transformations, the controlling equations are transformed into dimensionless ordinary differential equations. Numerical analysis was performed using bvp5c in MATLAB with a shooting technique. The results are demonstrated graphically and given a possible physical explanation for the velocity, temperature, and concentration profiles with respect to different parameters. Also, the numerical values for the Skin-friction coefficient, Nusselt number, and Sherwood number are presented in tabular form. It was observed that the velocity and temperature profiles increased and the concentration profile decreased with the increase in Indium Nitride nanoparticle volume fraction of the Williamson nanofluid. Relevant physical significances were also offered towards each observed result.

1. INTRODUCTION:

The study of Williamson fluids in porous media has attracted the attention of many researchers due to vast scientific developments in their applications. Williamson fluid is a non-Newtonian fluid with low viscosity and a high rate of shear stress. In other words, the effective viscosity of Williamson fluid should drop independently as the shear rate increases, which is nothing but infinite viscosity under no stress situation (stationary or no shear rate) and nil viscosity as the shear rate approach infinity.

Nanofluids are a modern class of fluids that consist of nanoparticles mixed with a basic fluid like water, Ethylene glycol, Propylene glycol, and oil. Nanoparticles are regarded as distinctive due to their possible thermophysical characteristics in typical base fluids. Choi [1] created the term nanofluids for the first time in 1995 and proposed that nanofluids may be classified as a new class of fluids used to enhance heat transfer mechanisms. Nanofluids are utilized in a variety of industrial applications due to their unique properties, such as coolants in nuclear reactors, heat exchangers, solar collectors, thermal reading over a flat surface, radiators, microelectronic systems, and so on. Xuan and Li [2] developed a detailed technique for manufacturing numerous nanofluids by directly combining nanophase particles with base fluids. Later, numerous researchers and scientists expanded on this notion to achieve spectacular results in flow and heat transmission [3]–[6]. All these investigations found that nanofluids were unable to offer the high heat transfer rates necessary for large-scale businesses. To compensate for this weakness, hybrid nanofluids are formed by mixing one or more distinct nanoparticles in a carrier fluid[7]. When compared to carrier fluids and nanofluids, these hybrid nanofluids will have better thermal properties. Gowda et al. [8] have investigated the flowing behavior of a hybrid nanofluid across a rotating disc in presence of activation energy[7]. Hossiany and Eid [9] investigated the heat transfer mechanism and flow of a propylene glycol-water-based fluid with hybrid nanoparticle suspension[7].

Fluid flow over a stretched sheet with heat transfer is crucial in terms of engineering and design applications. We can specifically pinpoint its uses: cooling of a metallic shield, plastic sheet extrusion, glass fiber production, wire drawing, polymer extrusion process, cooling shower, metal turning process, and so forth. Prasannakumara et al.[10] investigated the flow of fluids past a stretched sheet. Qayyum et al. [11],[12] investigated MHD nanofluid flow over a nonlinearly stretching sheet and studied the effect of viscous dissipation on the flow of a magnetized nanofluid on a curved stretching sheet[7]. Hayat et al. [13] described a mixed convective stream of fluid with carbon nanotubes flowing across an arched stretched sheet under the influence of a magnetic field[7]. Three-dimensional nanofluid flow under various conditions like thermal radiation over a nonlinearly stretching sheet with slip [14],[15], electromagnetic radiative non-Newtonian flow with Joule heating associated with chemical reactions in porous materials [16], hydro-magnetic convective and chemically reactive Williamson nanofluid with non-uniform heat absorption and

generation [17], the effect of variable thermal conductivity on nanofluid flow over a stretching sheet [18] were addressed and explained in terms of thermal diffusion of nanofluid.

Noor Muhammad and Sohail Nadeem [19] have studied the thermal behavior of base fluid Ethylene Glycol added with ferromagnetic nanoparticles like Fe_2O_4, $NiZnFe_2O_4$, and $MnZnFe_2O_4$ on stretching sheet under boundary conditions and compared the effects of magnetic dipole interactions on the fluid flow. Impacts of emerging parameters on the magneto-thermomechanical coupling are analyzed numerically. Muhammad Ramzan et al. [20] discussed the flow of Nanofluids consisting of $NiZnFe_2O_4$ nanoparticles and ethylene glycol over a curved surface to understand the heat transfer flow.

Summarily, researchers have studied the flow of nanofluids consisting of metallic (Cu, Ag, Au), nonmetallic (MgO, TiO2, Al_2O_3), ferrite (Fe_2O_3, $ZnFe_2O_3$, $CoFe_2O_3$) nanoparticles [21]–[26] under various other conditions like stretching sheet, inclined magnetic field, thermal flux, nonlinearly stretched porous sheet, etc. Water, transformer oil, ethylene glycol, and toluene have so far been identified as base fluids. The nanoparticles utilized may be divided into three types: pure metallic particles, ceramic particles, and carbon nanotubes (CNTs). Distinct combinations of the aforementioned particles and fluids result in different nanofluids. However, in this study, they will be classified mostly by particle type.

However, a study of Nanofluids consisting of inorganic semiconductor nanoparticles is not attempted except few studies on ZnO [27], [28] semiconductor nanoparticles. There are many semiconductor nanoparticles with high melting points (> 1000 ^oC) which may ensure no deviation in the bond strengths among the constituent atoms of nanoparticles. At the same time, these nanoparticles have good thermal properties like the convection of heat. Therefore, it is felt that the results on heat transfer of nanofluids consisting of semiconductor nanoparticles under different external forces and boundary conditions are interesting and useful. Hence the present analysis was attempted on Williamson fluid consisting of InN nanoparticles added with base fluid (water) and studied the effects of Magnetic field, radiation, and Arrhenius activation energy over a linearly stretched sheet with a porous medium to understand temperature, velocity, and concentration profiles. InN semiconductor compound nanoparticles nowadays are intensely used in the preparation of photo sensors, solar cells, and prominent electronic industries. In view of this, InN nanoparticles are mixed with the base fluid and studied for the heat flow effects.

2. MATHEMATICAL MODEL:

2.1 The governing equations:

To establish a mathematical model for a 3-dimensional boundary layer flow, a liquid flow under steady-state, laminar, incompressible viscous nanofluid past a stretching sheet is considered under the following assumptions.

1. The sheet is stretched laterally along x and y -axes with the velocity $u_w(x) = ax$, and $v_w(y) = by$ (a, b are stretching constants) respectively. Figure 1 shows the physical representation of the problem.
2. The sheet has a uniform surface temperature (T_w) and concentration (C_w) coinciding with the plane z=0, where the z-axis is perpendicular to the movement of the fluid with the flow confined to a half-plane of z > 0.
3. T_∞ and C_∞ represent ambient fluid temperature and concentration respectively (at its free surface).
4. Williamson nanofluid flow consists of InN nanoparticles of uniform shape and size and base fluid of water.
5. The magnetic field of uniform field strength B_o is applied normal to the stretched surface (kept in the XY plane) i.e. along the Z-direction.
6. Reynolds number of the fluid is considered to be small, therefore, the induced magnetic field in the fluid is neglected.
7. The pressure gradient along the linear stretched sheet is negligible ($\boldsymbol{\partial p/\partial x = 0}$).

The heat transport mechanism in Williamson nanofluid at par linearly stretched porous sheet applied with uniform magnetic field in presence of non-linear thermal radiation and activation energy is carried out. The thermophysical properties of nanoparticles and the base fluid considered in the present investigation are given in Table 1.

The model of Williamson fluid is taken [29], [30],[17] as

$$\dot{S} = -\dot{p}I + \tau, \tag{1}$$

$$\tau = [\mu_\infty + \frac{(\mu_0 - \mu_\infty)}{1-\Gamma\dot{\gamma}}]A_1, \tag{2}$$

The symbols in the above equations represent τ - extra stress tensor; S - Cauchy stress tensor; I - identity vector; p- pressure; μ_0 −limiting viscosity at zero shear rate; A_1 - first Rivlin-Erickson tensor; μ_∞- limiting viscosity at infinity shear rate; $\Gamma > 0$ - time constant;

$$\dot{\gamma} = \sqrt{\{\frac{1}{2} trace\ (A_1^2)\}}, \tag{3}$$

Here, they are all measured in the case of

$\mu_\infty = 0$ and $\Gamma\dot{\gamma} < 1$.

Thus, τ takes the form

$$\tau = [\frac{\mu_0}{1-\Gamma\dot{\gamma}}]A_1, \tag{4}$$

Applying binomial expansion to equation (4), we get

$$\tau = \mu_0[1 + \Gamma\dot{\gamma}]A_1. \tag{5}$$

The governing equations and the associated boundary conditions [17], [15],[31]–[33] are as follows

$$\frac{\partial u}{\partial x} + \frac{\partial v}{\partial y} + \frac{\partial w}{\partial z} = 0 \tag{6}$$

$$u\frac{\partial u}{\partial x}+v\frac{\partial u}{\partial y}+w\frac{\partial u}{\partial z}=\frac{\mu_{nf}}{\rho_{nf}}\frac{\partial^2 u}{\partial y^2}+\sqrt{2}\frac{\mu_{nf}}{\rho_{nf}}\Gamma\frac{\partial u}{\partial z}\frac{\partial^2 u}{\partial z^2}-\frac{\sigma {B_o}^2}{\rho_{nf}}u-\frac{\mu_{nf}}{\rho_{nf}K_p}u \quad (7)$$

$$u\frac{\partial v}{\partial x}+v\frac{\partial v}{\partial y}+w\frac{\partial v}{\partial z}=\frac{\mu_{nf}}{\rho_{nf}}\frac{\partial^2 v}{\partial y^2}+\sqrt{2}\frac{\mu_{nf}}{\rho_{nf}}\Gamma\frac{\partial v}{\partial z}\frac{\partial^2 v}{\partial z^2}-\frac{\sigma {B_o}^2}{\rho_{nf}}v-\frac{\mu_{nf}}{\rho_{nf}K_p}v \quad (8)$$

$$u\frac{\partial T}{\partial x}+v\frac{\partial T}{\partial y}+w\frac{\partial T}{\partial z}=\alpha_{nf}\frac{\partial^2 T}{\partial y^2}-\frac{1}{(\rho c_p)_{nf}}\frac{\partial q_r}{\partial z} \quad (9)$$

$$u\frac{\partial C}{\partial x}+v\frac{\partial C}{\partial y}+w\frac{\partial C}{\partial z}=D_B\frac{\partial^2 C}{\partial y^2}-K_o^2(c-c_\infty)\left(\frac{T}{T_\infty}\right)^m\exp\left(\frac{-E_a}{kT}\right) \quad (10)$$

By Rosseland approximation, the radiative heat flux $\frac{\partial q_r}{\partial z}$ [16] is given by $\frac{\partial q_r}{\partial z}=\frac{16\,\sigma^* T_\infty^3}{3\,k^*}\frac{\partial^2 T}{\partial z^2}$

2.2 Boundary conditions

According to Geethan Kumar [17] the boundary conditions for the velocity, temperature, and concentration fields are:

$$z=0: \quad u=u_w, \quad v=v_w, \quad w=0, \quad -K\frac{\partial T}{\partial z}=h_f(T_w-T), \quad C\to C_w$$

$$z\to\infty: \quad u\to 0, \quad v\to 0, \quad T\to T_\infty \quad C\to C_\infty \quad (11)$$

where h_f represents the heat transfer coefficient and K the thermal conductivity.

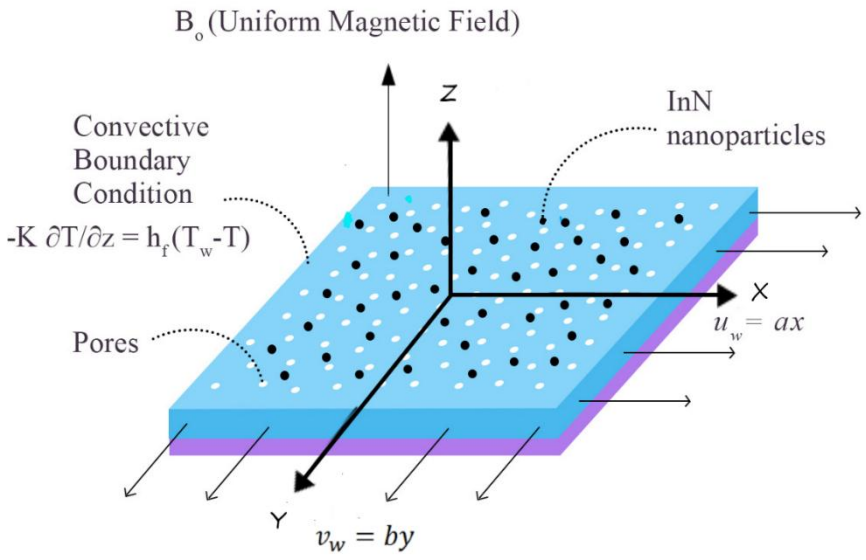

Fig. 1: Diagrammatic representation of the problem

Table 1: *Thermophysical properties of the fluid and nanoparticles*

Physical parameters	Water (H_2O) [34]	Indium Nitride (InN) [35], [36]
P (kg/m^3)	997.1	4250
Cp (J/kgK)	4179	686.2
k (W/mK)	0.613	8.954

The mathematical expressions for different thermophysical properties of nanofluid are given below in Table 2

Table 2: *Mathematical equations of thermophysical properties of nanofluid* [21]**,**[37]

Properties	***Equation(s***
Thermal Diffusivity	$\alpha_{nf} = \frac{k_{nf}}{(\rho c_p)_{nf}}$,
Dynamic Viscosity	$\mu_{nf} = \frac{\mu_f}{(1-\Phi)^{2.5}}$,
Thermal conductivity	$K_{nf} = K_f \left(\frac{K_s+2K_f-2\Phi(K_f-K_s)}{K_s+2K_f+\Phi(K_f-K_s)}\right)$
Density	$\rho_{nf} = (1-\Phi)\rho_f + \Phi\rho_s$
Heat capacity	$(\rho C_p)_{nf} = (1-\Phi)(\rho C_p)_f + \Phi(\rho C_p)_s$
Kinematic viscosity	$\nu_f = \frac{\mu_f}{\rho_f}$

2.3 Similarity equations

The similarity equations are used to transform the governing equations (7) to (10) into a set of ordinary differential equations by considering the three-dimensional linear similarity transformations

$$u = axf'(\eta), \quad v = ayg'(\eta), \quad w = -\sqrt{p\nu_f}(f(\eta)+g(\eta))$$

$$\theta(\eta) = \frac{T-T_\infty}{T_w-T_\infty}, \qquad \eta = z\sqrt{a/\nu_f}, \qquad \emptyset(\eta) = \frac{C-C_\infty}{C_w-C_\infty} \tag{12}$$

In terms of the above equations, the continuity equation (6) is satisfied whereas the equations (7) – (10) are transformed to second and third-order ordinary differential equations given below.

$$(1+\left((1-\Phi)+\Phi\Phi_1\right)(1-\Phi)^{2.5}\lambda_1 f'')f''' = \left((1-\Phi)+\Phi\Phi_1\right)(1-\Phi)^{2.5}(f'^2-(f+g)f'') + Mf'(1-\Phi)^{2.5} + Kf' \tag{13}$$

$$(1+\left((1-\Phi)+\Phi\Phi_1\right)(1-\Phi)^{2.5}\lambda_2 g'')g''' = \left((1-\Phi)+\Phi\Phi_1\right)(1-\Phi)^{2.5}(g'^2-(f+g)g'') + Mg'(1-\Phi)^{2.5} + Kg' \tag{14}$$

$$\left(\frac{k_{nf}}{k_f}+\frac{4}{3R}\right)\theta'' = -Pr\,(f+g)\,\theta'((1-\Phi)+\Phi\Phi_2) \tag{15}$$

$$\emptyset'' = -(Sc)\left(\sigma\,\emptyset\,(\theta\delta+1)^m \exp\left(\frac{-E}{1+\delta\theta}\right) - \emptyset'(f+g)\right) \tag{16}$$

Here $f, g, \emptyset, \theta$ *are the functions of* η and $\Phi_1 = \frac{\rho_s}{\rho_f}$, $\Phi_2 = \frac{(\rho C_p)_s}{(\rho C_p)_f}$

The corresponding boundary conditions are

$$at \quad \eta = 0: \quad f'(\eta) = 1, \quad f(\eta) = 0, \quad g(\eta) = 0, \quad g'(\eta) = \propto, \quad \theta'(\eta) = -Bi(1-\theta(\eta)), \quad \emptyset(\eta) = 1$$

$$at \quad \eta \to \infty: \quad f'(\eta) \to 0, \quad g'(\eta) \to 0 \qquad \theta(\eta) \to 0, \qquad \emptyset(\eta) \to 0 \tag{17}$$

where prime denotes the differentiation with respect to η. The associated non-dimensional parameters are

$$\lambda = \Gamma x\sqrt{a^3/2\nu}, \quad \lambda_1 = \Gamma y\sqrt{a^3/2\nu}, \quad M = \frac{\sigma B_o^2}{\rho_f a}, \quad P_r = \frac{(\rho c_p)_f \nu_f}{K_f}, \quad S_c = \frac{\nu_f}{D_B}, \quad R = \frac{4\sigma^* T_\infty^3}{k^* K_f}, \alpha = \frac{b}{a}, \quad \delta = \frac{T_w-T_\infty}{T_\infty}, \sigma = \frac{K_o^2}{a}, \quad E = \frac{E_a}{kT_\infty} \tag{18}$$

Interesting physical quantities in this problem are the heat transfer rates i.e., Nusselt numberNu, the Skin-friction coefficient C_f , and Sherwood number S_h (see for example [20][33]) are defined as

$$C_{fx} = \frac{\tau_{xz}}{\left(\frac{1}{2}\rho_f u_w^2\right)}, \qquad C_{fy} = \frac{\tau_{yz}}{\left(\frac{1}{2}\rho_f v_w^2\right)},$$

$$Nu = \frac{-x\,q_w}{(T_w-T_\infty)} \qquad \text{and} \quad S_h = \frac{-xJ_w}{(C_w-C_\infty)} \tag{19}$$

Here, $\tau_{xz} = \mu_{nf}\left[\frac{\partial u}{\partial z} + \frac{\Gamma}{\sqrt{2}}\left(\frac{\partial u}{\partial z}\right)^2\right]_{z=0}$, $\tau_{yz} = \mu_{nf}\left[\frac{\partial v}{\partial z} + \frac{\Gamma}{\sqrt{2}}\left(\frac{\partial v}{\partial z}\right)^2\right]_{z=0}$

represent shear stress at the surface,

$q_w = -\left[k + \frac{16\,\sigma^* T_\infty^3}{3\,k^*}\right]\left(\frac{\partial T}{\partial z}\right)_{z=0}$ is the wall heat, and

$$J_w = -D\left(\frac{\partial C}{\partial z}\right)_{z=0} \tag{20}$$

is the mass transfer.

By using equations (19), (20) the dimensionless Skin-friction coefficient, Nusselt number, and Sherwood number[38][39][40][41] are simplified as

$$\left.\begin{aligned} 2(Re_x)^{1/2}\,C_{fx} &= \frac{1}{(1-\Phi)^{2.5}}\left[f''(0)+\frac{\lambda}{2}(f''(0))^2\right] \\ 2(Re_x)^{1/2}\,C_{fy} &= \frac{1}{\propto^{3/2}(1-\Phi)^{2.5}}\left[g''(0)+\frac{\lambda}{2}(g''(0))^2\right] \\ (Re_x)^{-1/2}\,Nu_x &= -\left[\frac{k_{nf}}{k_f}+\frac{4}{3}R\right]\theta'(0) \\ (Re_x)^{-1/2}\,Sh &= -\emptyset'(0) \end{aligned}\right\} \tag{21}$$

$Re_x = \frac{u_w x}{\nu_f}$, $Re_y = \frac{v_w y}{\nu_f}$ are Reynold's numbers.

3. NUMERICAL METHOD AND VALIDATION:

Using the shooting approach, numerical answers are derived for the given non-dimensional equations. The MATLAB built-in bvp5c function is then used to confirm the acquired results. The missing beginning conditions are assumed in the firing technique and guided towards the boundary conditions using the RK-4 order method. The numerical bvp5c produced from the notion of a finite-difference scheme is used to compare the results.

$$f_1' = f_2, f_2' = f_3, and\ f_3' = \frac{((1-\Phi)+\Phi\Phi_1)(1-\Phi)^{2.5}({f_2}^2-(f_1+f_4)f_3)+Mf_2(1-\Phi)^{2.5}+K f_2}{(1+((1-\Phi)+\Phi\Phi_1)(1-\Phi)^{2.5}\lambda f_3)} \quad (22)$$

$$f_4' = f_5, f_5' = f_6, and\ f_6' = \frac{((1-\Phi)+\Phi\Phi_1)(1-\Phi)^{2.5}({f_5}^2-(f_1+f_4)f_6)+Mf_5(1-\Phi)^{2.5}+K f_5}{(1+((1-\Phi)+\Phi\Phi_1)(1-\Phi)^{2.5}\lambda f_6)} \quad (23)$$

$$f_7' = f_8, f_8' = -\frac{Pr\,(f_1+f_4)f_8\ ((1-\Phi)+\Phi\Phi_2)}{\left(\frac{k_f}{k_{nf}}+\frac{4}{3R}\right)} \quad (24)$$

$$f_9' = f_{10}, f_{10}' = (Sc)\left(\sigma\, f_9\,(f_7\delta+1)^m \exp\left(\frac{-E}{1+\delta f_7}\right) - (f_1+f_4)f_{10}\right) \quad (25)$$

The converted initial conditions are written as

$$f_2(0) = 1,\ f_1(0) = 0,\ f_4(0) = 0,\ f_5 = \propto,\ f_8 = -Bi(1-f_7),\ f_9 = 1$$
$$f_2 \to 0, \quad f_5 \to 0, \quad f_7 \to 0, \quad f_9 \to 0$$

The governed equations (7) – (10) with boundary conditions (11) are tedious to solve analytically, they are solved numerically in MATLAB using the bvp5c approach. The computations are initialized based on fixed values of physical parameters λ_1=λ_2=0.2, σ=E=δ=1.0, Sc=0.6, Pr=6.2, R=K=M=Bi=α=0.5. The same base values may be assumed for the entire investigation as long as there is no particular indication. Finally, as a part of the validation of our computations, the cross-check of these results with the solutions of Ariel [42] and Geethan et al. [17] (see Table 3) is made and found that the results are in close agreement. Error tolerance of 10^{-5} is applied during the calculations, and all results are accurate within the set tolerance.

Table 3: *Comparison of results of Skin friction coefficients ($C_f\,Re_x^{1/2}$, $-C_f\,Re_y^{1/2}$) for different values of α when M = K = λ_1 = λ_2 = Φ = 0.*

α	**Present result**	**Present result**	**Ariel** [42]		**Geethan et al.** [17]	
	$-C_f\,Re_x^{1/2}$	$-C_f\,Re_y^{1/2}$	$-C_f\,Re_x^{1/2}$	$-C_f\,Re_y^{1/2}$	$-C_f\,Re_x^{1/2}$	$-C_f\,Re_y^{1/2}$
0	1	0	1	0	1.000003	0
0.1	1.020264	0.066849	1.02025978	0.06684715	1.020265	0.066849
0.2	1.039497	0.148738	1.03949519	0.14873691	1.039498	0.148738
0.3	1.057956	0.243361	1.05795478	0.24335980	1.057957	0.243361
0.4	1.075788	0.349209	1.07578811	0.34920865	1.075789	0.349209
0.5	1.093096	0.465205	1.09309502	0.46520485	1.093096	0.465205
0.6	1.109947	0.590529	1.10994694	0.59052892	1.109948	0.590526
0.7	1.126398	0.724532	1.12639752	0.72453174	1.126399	0.724528
0.8	1.142489	0.866683	1.14248862	0.86668292	1.142490	0.866679
0.9	1.158254	1.016539	1.15825383	1.01653870	1.158255	1.016535
1	1.173721	1.173721	1.17372074	1.17372074	1.173722	1.173717

4. RESULTS AND DISCUSSION:

Figures 2 to Figure 25 are graphical representations of several flow characteristics used to estimate momentum, energy, and mass species [27]. Table 4 and 5 also show the numerical values of skin friction coefficients, as well as the rate of heat and mass transfer coefficients [27].

Table 4: *Numerical data of Skin friction coefficient, Nusselt number, and Sherwood number*[38]

M	K	λ_1	λ_2	α	Φ	$-C_f\,Re_x^{1/2}$	$-C_f\,Re_y^{1/2}$	$Re_x^{-1/2}Nu$	$Re_x^{-1/2}\,Sh$
0.5	0.5	0.2	0.2	0.5	0.1	1.922696	0.884977	0.720555	0.913338
1						2.072316	0.967959	0.715893	0.907305
1.5						2.212567	1.044399	0.711392	0.902049
2						2.345457	1.115553	0.707027	0.897414
	1					2.115468	0.991618	0.714521	0.905647
	1.5					2.293425	1.087852	0.708746	0.899189
	2					2.460727	1.176098	0.703181	0.893658
		0.1				1.950935	0.887464	0.722520	0.915872

		0.3				1.930052	0.881303	0.717573	0.909754
		0.4				1.372094	0.876082	0.713106	0.904745
			0.1			1.923476	0.891063	0.720939	0.913842
			0.3			1.921824	0.879086	0.720126	0.912783
			0.4			1.920832	0.873693	0.719637	0.912162
				0.1		1.851194	0.153731	0.682582	0.878303
				0.3		1.887777	0.498080	0.703977	0.896195
				0.7		1.955929	1.308172	0.733862	0.929599
					0.2	2.552057	1.165362	0.828356	0.917466
					0.3	3.340135	1.540953	0.959073	0.925480
					0.4	4.452383	2.088174	1.122203	0.936335

Table 5: *Numerical data of Skin friction coefficient, Nusselt number, and Sherwood number*[38]

R	Pr	Bi	Sc	E	δ	σ	m	$-C_f\,Re_x^{1/2}$	$-C_f\,Re_y^{1/2}$	$Re_x^{-1/2}Nu$	$Re_x^{-1/2}\,Sh$
0.5	6.2	0.5	0.6	0.3	1.0	1.0	1.0	1.922696	0.884977	0.720555	0.913338
1								1.922696	0.884977	0.911466	0.917248
1.5								1.922696	0.884977	1.087049	0.920643
2								1.922696	0.884977	1.250870	0.923573
	0.7							1.922696	0.884977	0.442850	0.942976
	4							1.922696	0.884977	0.661290	0.919470
	8							1.922696	0.884977	0.750847	0.910400
		1						1.922696	0.884977	1.131062	0.921525
		1.5						1.922696	0.884977	1.396207	0.926516
		2						1.922696	0.884977	1.581585	0.929882
			0.2					1.922696	0.884977	0.720555	0.536419
			0.4					1.922696	0.884977	0.720555	0.740009
			0.8					1.922696	0.884977	0.720555	1.065752
				0.5				1.922696	0.884977	0.720555	0.810263
				1.5				1.922696	0.884977	0.720555	0.642761
				2				1.922696	0.884977	0.720555	0.595008
					0.5			1.922696	0.884977	0.720555	0.905615
					1.5			1.922696	0.884977	0.720555	0.920555
					2			1.922696	0.884977	0.720555	0.927340
						0.5		1.922696	0.884977	0.720555	0.733332
						1.5		1.922696	0.884977	0.720555	1.064479
						2		1.922696	0.884977	0.720555	1.196774
							0.5	1.922696	0.884977	0.720555	0.921913
							1.5	1.922696	0.884977	0.720555	0.969093
							2	1.922696	0.884977	0.720555	0.995652

Figures 2-5 depict the impact of local Williamson parameters λ_1 and λ_2 on velocity, temperature, and concentration profiles parameter λ_1 rises, the axial velocity falls while the transverse velocity increases (see fig.2). In practice, the Williamson parameter is directly proportional to the relaxation time [17]; hence, the rise in the Williamson parameter corresponds to a rise in the ion relaxation time intern it generates an increase in fluid viscosity, which causes a decrease in velocity. With the impact of λ_2, a completely different trend is observed (see fig.3). As a result of increasing the Williamson parameter, the fluid velocity decreases, resulting in reduced heat transfer in the fluid. As a result, the fluid temperature rises and the same can be seen in figure 4. Williamson parameter causes the growth of viscosity of the nanofluid, thereby the concentration flow of

InN nanoparticles increases (Fig. 5).

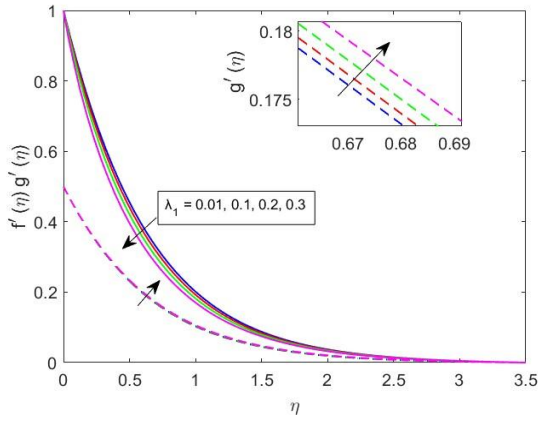

Fig. 2: Role of λ_1 on velocity profiles

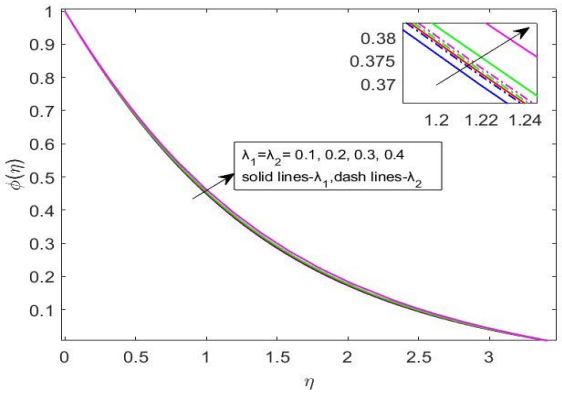

Fig. 5: Role of λ_1 & λ_2 on concentration profiles

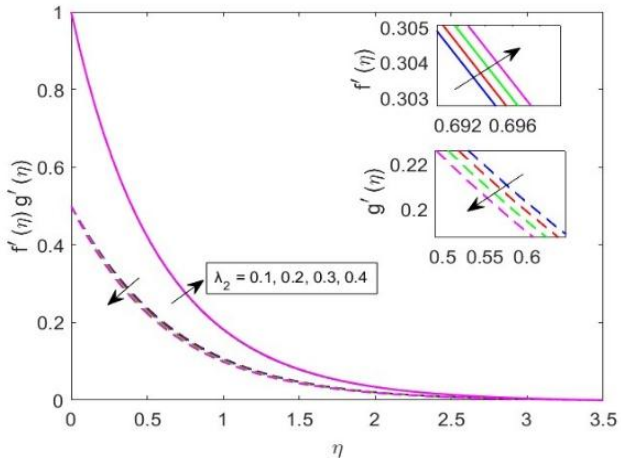

Fig. 3: Role of λ_2 on velocity profiles

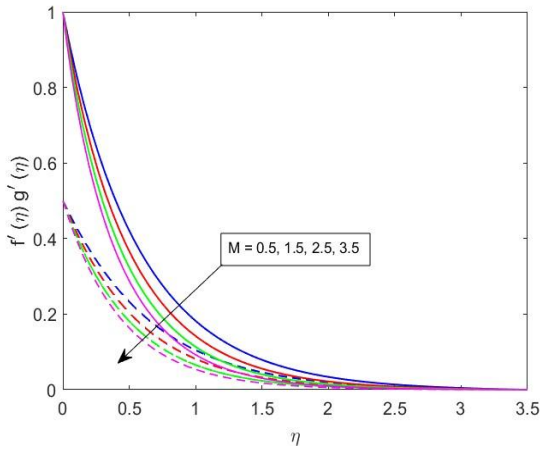

Fig. 6: Role of *M* on velocity profiles.

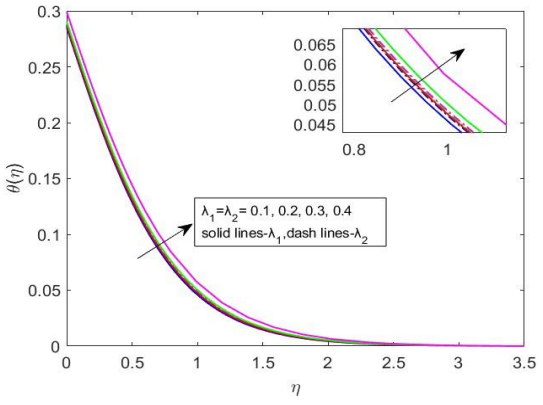

Fig. 4: Role of λ_1 & λ_2 on temperature profiles

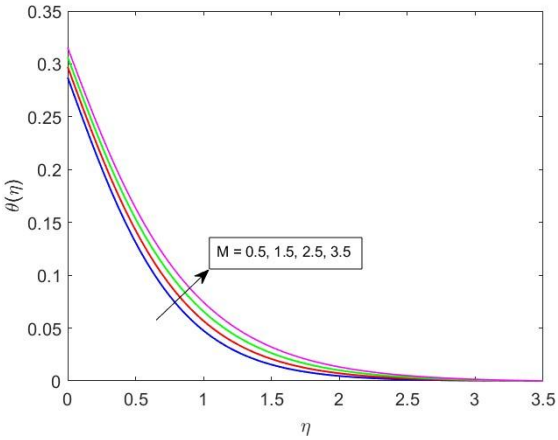

Fig. 7: Role of *M* on temperature profiles

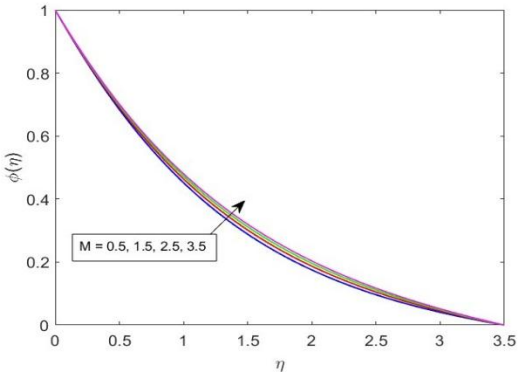

Fig. 8: Role of *M* on concentration profiles.

Figure 6 shows the reduced velocities of both axial and transverse with the increase in Magnetic field. This is because of the Lorentz force that arises with the increase in the applied magnetic field and this force resists the fluid flow and causes a reduction in both the velocities. Also, Lorentz forces cause internal friction among the particles in the fluid hence fluid temperature increases with the applied magnetic field [17] The temperature and concentration profiles of InN + water nanofluid are shown in Figure 7 and 8. The graphs indicate the temperature rise also causes a rise in concentration.

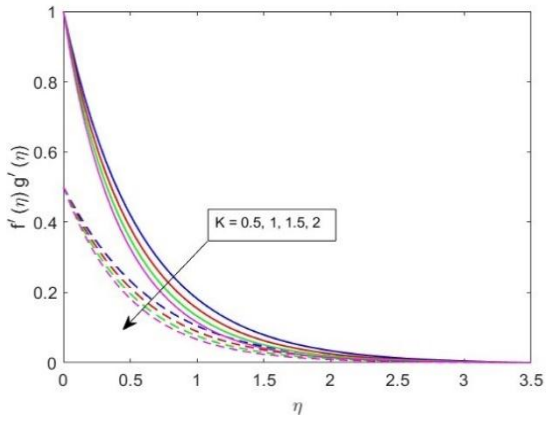

Fig. 9: Role of *K* on velocity profiles

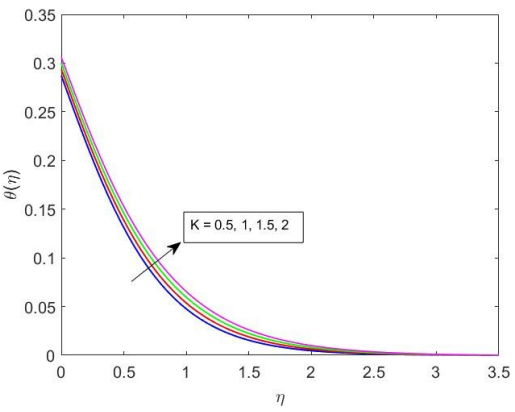

Fig. 10: Role of *K* on temperature profiles

It can be seen from Fig. 9 that as the porosity parameter increases, the axial and transverse velocities, as well as the related momentum boundary layer thickness, decrease. This is because increasing porosity generates higher fluid permeability in the Z-direction, which increases fluid velocity in this direction i.e. –ve Z-direction in particular. As a result, both fluid flow velocities are reduced. The porosity parameter, on the other hand, produces a rise in temperature and concentration. Figures 10 and 11 show this clearly in the case of fluid containing InN nanoparticles.

"The stretching rate parameter is the ratio of the transverse velocity to the axial velocity". In general, the porosity parameter reduces fluid velocity, resulting in high concentration. It signifies that the increase in a porous sheet's stretching parameter shows that the transverse velocity outnumbers the axial velocity [17]. Henceforth, the rise in the value of α causes a rise in the transverse velocity and simultaneously, a decrease in the axial velocity. This trend is clearly shown in Fig. 12. The stretching rate parameter α, also causes a decrease in the temperature and concentration profile (Fig 13, 14).

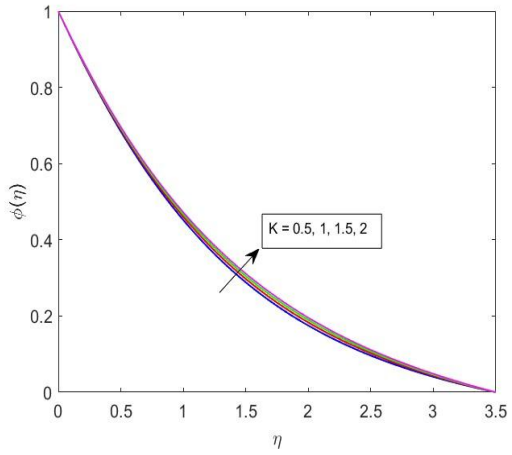

Fig. 11: Role of *K* on concentration profiles

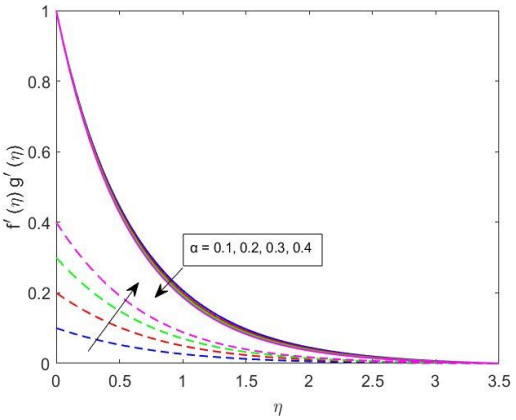

Fig.12: Role of α on velocity profiles

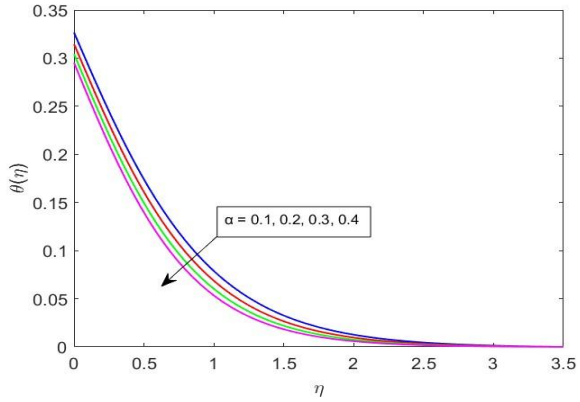

Fig. 13: Role of α on temperature profiles

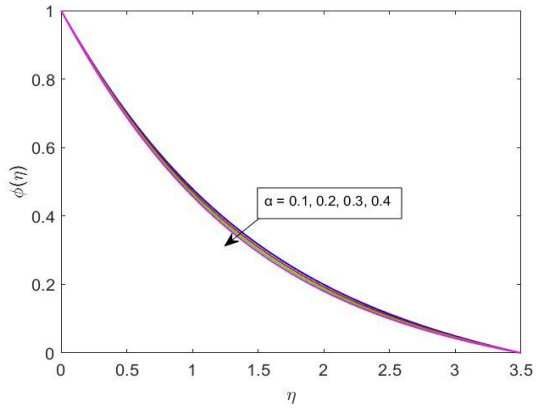

Fig. 14: Role of α on concentration fields

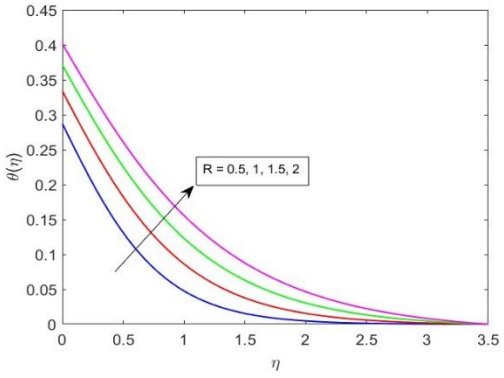

Fig. 15: Role of R on temperature profiles.

Thermal radiation, the strength of which is represented in terms of radiation parameter R, applied to a nanofluid, enhances the fluid temperature and boundary layer thickness with the increase in parameter R. This result, observed in the nanofluid consisting of InN nanoparticles mixed with water is shown clearly in Figure 15. Thermal radiation adds heat to the working fluid, causing the fluid temperature to rise. It is worth mentioning that the concentration field decreases with the increase in thermal radiation (Fig.16) as a result of the random movement of fluid molecules.

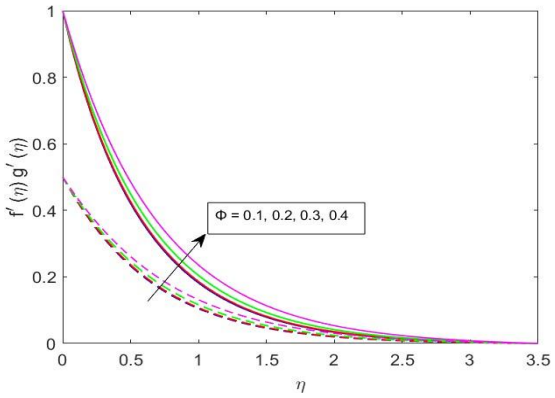

Fig. 16: Role of Φ on velocity profile

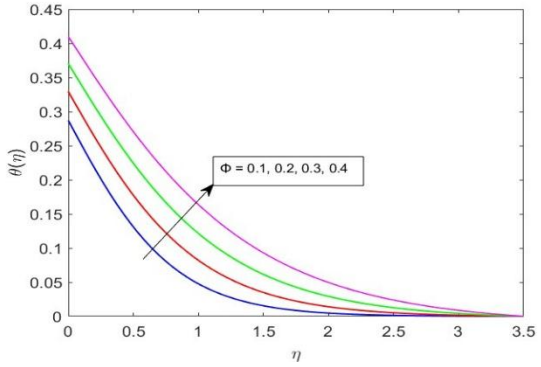

Fig. 17: Role of Φ on temperature profile

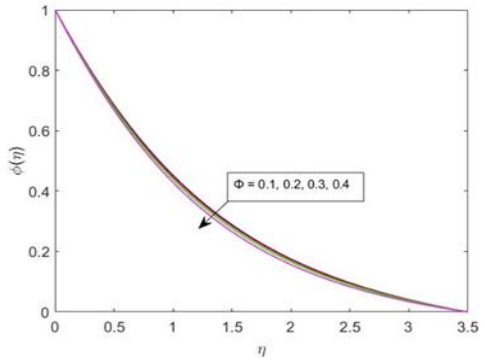

Fig. 18: Role of Φ on concentration profile

Figures 16,17, and 18 show the characterization of the nanofluid volume fraction at different velocities, temperatures, and concentrations. It is observed that when Φ increases, so does the velocity profile along the axial and transverse axes (Fig. 16). With the same order of Φ, the resistance force within the fluid increases, while the temperature profiles exhibit opposite behavior (Fig.17). This is because the thermal conductivity and thickness of the thermal boundary layer decrease as Φ increases. A similar result was also observed in Al2O3-water nanofluids by Hammed Abiodun Ogunseye et al.

[43]. It is obvious from Fig.18 that the concentration profile of InN-water nanofluid decreases. A similar observation was also made by Kandasamy[44] in SWCNT-water nanofluids. According to them the observed decrease in concentration profile is due to the stronger diffusion boundary layer thickness that the SWCNT-water nanofluids have when compared to Cu-water fluids since the carbon nanotubes have extraordinary mechanical, electrical, thermal, optical, and chemical properties[44]. Nanofluid, under the present study, has InN nanoparticles of very good optical, electrical and chemical properties, by virtue of the nitride present in the compound, the fluid may also be assigned with strong diffusion boundary layer thickness responsible for the decrease in the concentration profile.

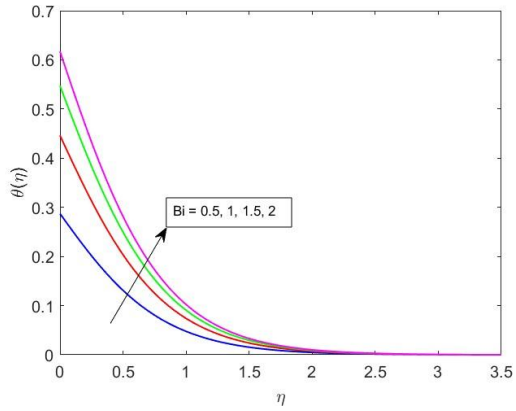

Fig. 19: Role of *Bi* on temperature Profile

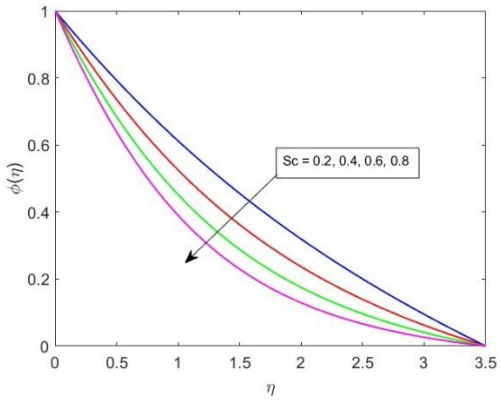

Fig. 20: Role of *Sc* on concentration profile

The temperature profile of InN-water nanofluid accelerates with increasing thermal Biot number *Bi* and the same is noted in Fig.19. In general, the thermal Biot number describes convection. As the Biot number grows convection improves. As a result of the increasing thermal Biot number, the fluid temperature increases. Fig.20 depicts the graphical variation between species concentration and Schmidt number Sc. It is obvious from the figure that the nanoparticle concentration decreases with the increase in Sc. This is because the Schmidt number varies inverse proportion to the rate of diffusion of mass [17]. Therefore, diffusion of mass decreases as the Schmidt number increases.

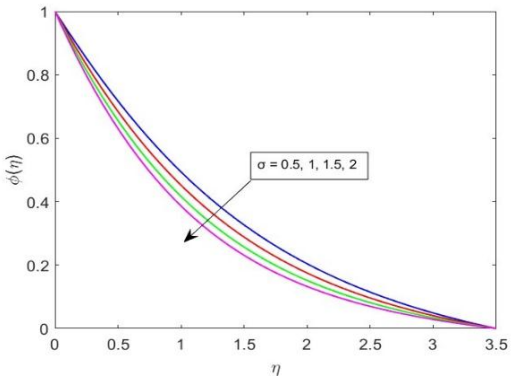

Fig. 21: Role of σ on concentration profile

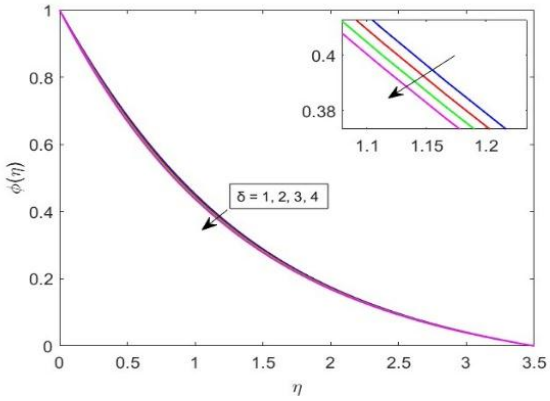

Fig. 22: Role of ***δ*** on concentration profile

According to Fig. 21, the species (InN nanoparticles) concentration falls as the boundary layer thickness of the solute (water) decreases as a result of an increase in chemical reaction parameter. Practically, the diffusivity of the fluid varies due to changes in the intensity of the chemical reaction, and thus the concentration declines. Kandasamy et al. [44] discovered that when the chemical reaction and buoyancy ratio increased, the concentration of water-based SWCNTs, Cu, and Al_2O_3 decreased, but the rate of mass transfer increased due to the combined impact of diffusion conductivity and kinematic viscosity of the nanoparticles. They also discovered that the diffusion boundary layer thickness of water-base Cu and SWCNTs increases faster than that of Al_2O_3-water as the chemical reaction progresses [44].

Figure 22 explores the effect of temperature difference parameter δ on the concentration field of InN-water nanofluid. The temperature difference parameter δ is defined as the difference between surface and ambient temperatures. When δ grows, the concentration boundary layer thickness increases, resulting in a decrease in the concentration field. A similar observation i.e. decrease of concentration field as a result of an increase in δ was also made on Maxwell-Sutterby fluid by Sajid et al. [34].

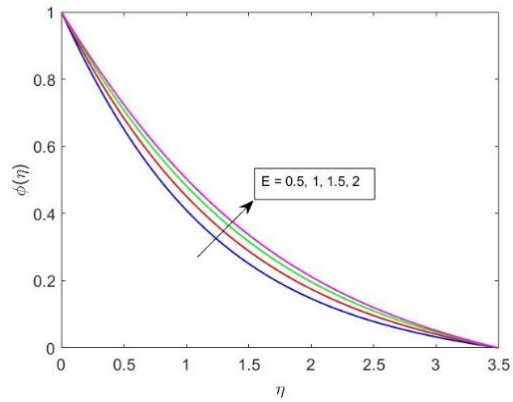

Fig. 23: Role of *E* on concentration profile

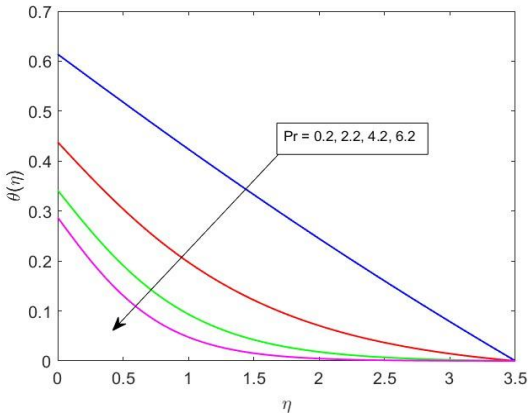

Fig. 24: Role of *Pr* on concentration profile

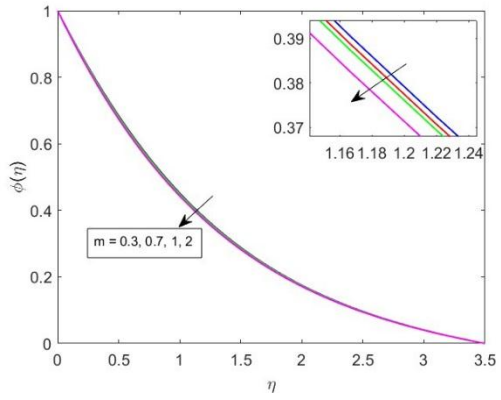

Fig. 25: Role of *m* on concentration profile

The impact of Arrhenius activation parameter *E* on the concentration profiles of InN-water nanofluid is illustrated in Fig.23. Truly, *E* is the energy that must be used to proceed with the chemical reaction. It is also defined as the least amount of energy necessary to initiate and sustain a chemical reaction. It is a general observation that the increase in the activation energy causes an increase in the nanoparticle concentration. Aamir Hamid et al. [45] have studied the "Impacts of chemical reaction with activation energy on the unsteady flow of magneto-Williamson nanofluids" and concluded that an increase in the destructive chemical reaction parameter $\boldsymbol{\sigma} > 0$ tends to reduce the nanoparticle concentration profile[45]. The simulated concentration profiles for various temperature difference parameter δ were also studied in the presence and absence of a magnetic field and concluded that the concentration profile curves perceived a decaying behavior with higher values of temperature difference parameter and a general trend of increase in the nanoparticle concentration profile with the rise in activation energy *E* [45].

Figure 24 is drawn to understand the influence of Prandtl number *Pr* on the temperature profiles of InN-water nanofluid. "Prandtl number *Pr* is defined as the ratio of momentum diffusivity to the thermal diffusivity". According to the fundamental definition of Pr, increasing thermal diffusivity results in a decrease in Prandtl number, which depreciates the temperature field [34]

This type of behavior appears to be common in most of the nanofluids because several research articles on nanofluids with different nanoparticles in different base fluids appear in the literature [27][46], [47]. Figure 25 depicts the influence of the fitted rate constant m on the concentration profile of InN-water nanofluid. This graph demonstrates that the concentration profiles decrease with the increase in the fitted rate constant. Exactly a similar behavior was recorded in Maxwell-Sutterby fluid by Sajid et al. [34] wherein they showed an increase in mathematical factors that favors the destructive chemical reaction and leads to decrease the nanoparticle concentration profile.

5. CONCLUSIONS:

In this paper, a numerical analysis of a 3-D Williamson MHD fluid embedded with Indium Nitride semiconductor nanoparticles over a linearly stretching porous sheet with radiation and Arrhenius activation energy was presented. Numerical data of Skin friction coefficient, Nusselt number, and Sherwood numbers were used for the analysis, and MATLAB built-in *bvp4c* function was utilized for the confirmation of obtained results. The results presented in the paper are

1. A rise in the axial velocities and decrease in the transverse velocities with Williamson constants λ_1 and exactly a reverse effect with Williamson constants λ_2 were observed. The temperature and concentration profiles increase with the increase in Williamson fluid parameters.
2. Both axial and transverse velocities decrease whereas the temperature and concentration profiles increase with the increase in Magnetic field and porosity parameter.
3. Axial/transverse velocities decrease/increase and temperature & concentration profiles decrease with the increase in stretching ratio parameter.
4. The temperature profile showed a rising phenomenon with the increase in radiation parameter.

5. velocity and temperature profiles increase and the concentration profile decreases with the increase in volume fraction.
6. The temperature profile increases with an increase in Biot number and decreases with an increase in Prandtl number.
7. The concentration profile decreases with an increase in Schmidt number, fitted rate constant, and chemical reaction & temperature difference parameters.
8. The concentration profile increases with an increase in the Activation energy parameter.

NOMENCLATURE:

τ	extra stress tensor
S	Cauchy stress tensor
I	identity vector
P	pressure;
μ_0	limiting viscosity at zero shear rate;
A_1	first Rivlin- Erickson tensor;
μ_∞	Limiting viscosity at infinity shear rate
Γ	Time constant
ρ_{nf}	Nanofluid density
σ	Electric conductivity,
B_o	Magnetic field strength
μ_{nf}	Dynamic viscosity of the nanofluid
T	Temperature of the fluid
C	Concentration of the fluid
α_{nf}	Thermal diffusivity
D_B	Diffusion coefficient
K_p	Permeability of the porous medium
c_p	Specific heat at constant pressure
σ^*	Stefan Boltzmann constant
k^*	Mean absorption coefficient
α_{nf}	Thermal diffusivity
K_o	Chemical reaction constant
E_a	Activation energy parameter
k	Boltzmann constant
m	Fitted rate constant
Γ	Williamson fluid parameter
ρ	Density
λ_1 & λ_2	− Williamson parameters
M	Magnetic parameter
P_r	Prandtl number
S_c	Schmidt number
R	Radiation parameter
$\propto$	Stretching ratio parameter
δ	Temperature difference parameter
σ	Chemical reaction parameter
E	Activation energy parameter

ACKNOWLEDGEMENTS:

The authors would like to thank the Head, Department of Mathematics, University College of Science, Osmania University, Hyderabad, India for his participation in the discussions and help. One of the authors M. Jyotshna thanks the Principal and Head, Department of Applied Sciences and Humanities, *Maturi Venkata Subba Rao Engineering College*, Nadergul, Hyderabad for their constant encouragement and support in conduting the research work.

Conflicts of interest: The author declares no conflict of interest.

REFERENCES:

[1] Stephen U.S. Choi and J.A.Eastman, "ENHANCING THERMAL CONDUCTIVITY OF FLUIDS WITH NANOPARTICLES," *ASME International Mechanical Engineering Congress & Exposition*, vol. 231. 1995. doi: 10.1021/je60018a001.

[2] Y. Xuan and Q. Li, "Heat transfer enhancement of nanofluids," *Int. J. Heat Fluid Flow*, vol. 21, no. 1, pp. 58–64, 2000, doi: 10.1016/S0142-727X(99)00067-3.

[3] M. R. Eid, "Effects of NP Shapes on Non-Newtonian Bio-Nanofluid Flow in Suction/Blowing Process with Convective Condition: Sisko Model," *J. Non-Equilibrium Thermodyn.*, vol. 45, no. 2, pp. 97–108, 2020, doi: 10.1515/jnet-2019-0073.

[4] M. J. Kotresh, G. K. Ramesh, V. K. R. Shashikala, and B. C. Prasannakumara, "Assessment of Arrhenius activation energy in stretched flow of nanofluid over a rotating disc," *Heat Transf.*, vol. 50, no. 3, pp. 2807–2828, 2021, doi: 10.1002/htj.22006.

[5] M. Sheikholeslami, S. A. Shehzad, Z. Li, and A. Shafee, "Numerical modeling for alumina nanofluid magnetohydrodynamic convective heat transfer in a permeable medium using Darcy law," *Int. J. Heat Mass Transf.*, vol. 127, pp. 614–622, 2018, doi: 10.1016/j.ijheatmasstransfer.2018.07.013.

[6] M. R. Eid and A. F. Al-Hossainy, "Synthesis, DFT calculations, and heat transfer performance large-surface TiO2: ethylene glycol nanofluid and coolant applications," *Eur. Phys. J. Plus*, vol. 135, no. 7, 2020, doi: 10.1140/epjp/s13360-020-00599-y.

[7] H. B. Mallikarjuna, T. Nirmala, R. J. Punith Gowda, R. Manghat, and R. S. Varun Kumar, "Two-dimensional Darcy–Forchheimer flow of a dusty hybrid nanofluid over a stretching sheet with viscous dissipation," *Heat Transf.*, vol. 50, no. 4, pp. 3934–3947, 2021, doi: 10.1002/htj.22058.

[8] P. G. R. Jayadevamurthy, N. kumar Rangaswamy, B. C.

Prasannakumara, and K. S. Nisar, "Emphasis on unsteady dynamics of bioconvective hybrid nanofluid flow over an upward–downward moving rotating disk," *Numer. Methods Partial Differ. Equ.*, no. November, pp. 1–22, 2020, doi: 10.1002/num.22680.

[9] A. F. Al-Hossainy and M. R. Eid, "Structure, DFT calculations and heat transfer enhancement in [ZnO/PG + H2O]C hybrid nanofluid flow as a potential solar cell coolant application in a double-tube," *J. Mater. Sci. Mater. Electron.*, vol. 31, no. 18, pp. 15243–15257, 2020, doi: 10.1007/s10854-020-04089-w.

[10] B. C. Prasannakumara, B. J. Gireesha, M. R. Krishnamurthy, and K. Ganesh Kumar, "MHD flow and nonlinear radiative heat transfer of Sisko nanofluid over a nonlinear stretching sheet," *Informatics Med. Unlocked*, vol. 9, no. August, pp. 123–132, 2017, doi: 10.1016/j.imu.2017.07.006.

[11] S. Qayyum, M. I. Khan, W. Chammam, W. A. Khan, Z. Ali, and W. Ul-Haq, "Modeling and theoretical investigation of curved parabolized surface of second-order velocity slip flow: Combined analysis of entropy generation and activation energy," *Mod. Phys. Lett. B*, vol. 34, no. 33, pp. 1–15, 2020, doi: 10.1142/S0217984920503832.

[12] S. Qayyum, T. Hayat, and A. Alsaedi, "Thermal radiation and heat generation/absorption aspects in third grade magneto-nanofluid over a slendering stretching sheet with Newtonian conditions," *Phys. B Condens. Matter*, vol. 537, no. October 2017, pp. 139–149, 2018, doi: 10.1016/j.physb.2018.01.043.

[13] T. Hayat, M. Z. Kiyani, A. Alsaedi, M. Ijaz Khan, and I. Ahmad, "Mixed convective three-dimensional flow of Williamson nanofluid subject to chemical reaction," *Int. J. Heat Mass Transf.*, vol. 127, pp. 422–429, 2018, doi: 10.1016/j.ijheatmasstransfer.2018.06.124.

[14] C. Y. Wang, "The three-dimensional flow due to a stretching flat surface," *Phys. Fluids*, vol. 27, no. 8, pp. 1915–1917, 1984, doi: 10.1063/1.864868.

[15] B. Mahanthesh, B. J. Gireesha, R. S. R. Gorla, and O. D. Makinde, "Magnetohydrodynamic three-dimensional flow of nanofluids with slip and thermal radiation over a nonlinear stretching sheet: a numerical study," *Neural Comput. Appl.*, vol. 30, no. 5, pp. 1557–1567, 2018, doi: 10.1007/s00521-016-2742-5.

[16] A. A. Alaidrous and M. R. Eid, "3-D electromagnetic radiative non-Newtonian nanofluid flow with Joule heating and higher-order reactions in porous materials," *Sci. Rep.*, vol. 10, no. 1, pp. 1–19, 2020, doi: 10.1038/s41598-020-71543-4.

[17] K. S. Geethan, S. V. K. Varma, R. V. M. S. S. Kiran Kumar, C. S. K. Raju, S. A. Shehzad, and M. N. Bashir, "Three-dimensional hydromagnetic convective flow of chemically reactive williamson fluid with non-uniform heat absorption and generation," *Int. J. Chem. React. Eng.*, vol. 17, no. 2, pp. 1–17, 2019, doi: 10.1515/ijcre-2018-0118.

[18] T. Nainaru, P. V. S. Narayana, and B. Venkateswarlu, "Numerical simulation of variable thermal conductivity on 3D flow of nanofluid over a stretching sheet," *Nonlinear Eng.*, vol. 9, no. 1, pp. 233–243, 2020, doi: 10.1515/nleng-2020-0011.

[19] N. Muhammad and S. Nadeem, "Ferrite nanoparticles Ni- ZnFe2O4 , Mn- ZnFe2O4 and Fe2O4 in the flow of ferromagnetic nanofluid," *Eur. Phys. J. Plus*, vol. 132, no. 9, 2017, doi: 10.1140/epjp/i2017-11650-2.

[20] M. Ramzan, H. Gul, and M. Zahri, "Darcy-Forchheimer 3D Williamson nanofluid flow with generalized Fourier and Fick's laws in a stratified medium," *Bull. Polish Acad. Sci. Tech. Sci.*, vol. 68, no. 2, pp. 327–335, 2020, doi: 10.24425/bpasts.2020.133116.

[21] P. K. Kameswaran, P. Sibanda, and A. S. N. Murti, "Nanofluid flow over a permeable surface with convective boundary conditions and radiative heat transfer," *Math. Probl. Eng.*, vol. 2013, 2013, doi: 10.1155/2013/201219.

[22] N. Bachok, A. Ishak, and I. Pop, "Boundary layer stagnation-point flow and heat transfer over an exponentially stretching/shrinking sheet in a nanofluid," *Int. J. Heat Mass Transf.*, vol. 55, no. 25–26, pp. 8122–8128, 2012, doi: 10.1016/j.ijheatmasstransfer.2012.08.051.

[23] G. Mandal, "Convective-Radiative Heat Transfer of Micropolar Nanofluid Over a Vertical Non-Linear Stretching Sheet," *J. Nanofluids*, vol. 5, no. 6, pp. 852–860, 2016, doi: 10.1166/jon.2016.1265.

[24] S. Mandal and G. C. Shit, "Entropy analysis of unsteady MHD three-dimensional flow of Williamson nanofluid over a convectively heated stretching sheet," *Heat Transf.*, vol. 51, no. 2, pp. 2034–2062, 2022, doi: 10.1002/htj.22387.

[25] K. Swain and B. Mahanthesh, "Thermal Enhancement of Radiating Magneto-Nanoliquid with Nanoparticles Aggregation and Joule Heating: A Three-Dimensional Flow," *Arab. J. Sci. Eng.*, vol. 46, no. 6, pp. 5865–5873, 2021, doi: 10.1007/s13369-020-04979-5.

[26] A. A. Siddiqui and M. Sheikholeslami, "TiO2-water nanofluid in a porous channel under the effects of an inclined magnetic field and variable thermal conductivity," *Appl. Math. Mech. (English Ed.)*, vol. 39, no. 8, pp. 1201–1216, 2018, doi: 10.1007/s10483-018-2359-6.

[27] M. K. Nayak, J. Prakash, D. Tripathi, and V. S. Pandey, "3D radiative convective flow of ZnO-SAE50nano-lubricant in presence of varying magnetic field and heterogeneous reactions," *Propuls. Power Res.*, vol. 8, no. 4, pp. 339–350, 2019, doi: 10.1016/j.jppr.2019.10.002.

[28] N. A. Yacob, A. Dasman, and S. Ahmad, "Regional Conference on Science, Technology and Social Sciences (RCSTSS 2016)," *Reg. Conf. Sci. Technol. Soc. Sci. (RCSTSS 2016)*, no. Rcstss 2016, 2018, doi: 10.1007/978-981-13-0074-5.

[29] S. Nadeem, S. T. Hussain, and C. Lee, "Flow of a williamson fluid over a stretching sheet," *Brazilian J. Chem. Eng.*, vol. 30, no. 3, pp. 619–625, 2013, doi:

10.1590/S0104-66322013000300019.

[30] H. M. Shawky, N. T. M. Eldabe, K. A. Kamel, and E. A. Abd-Aziz, "MHD flow with heat and mass transfer of Williamson nanofluid over stretching sheet through porous medium," *Microsyst. Technol.*, vol. 25, no. 4, pp. 1155–1169, 2019, doi: 10.1007/s00542-018-4081-1.

[31] S. Bilal, Khalil-ur-Rehman, M. Y. Malik, A. Hussain, and M. Khan, "Effects of temperature dependent conductivity and absorptive/generative heat transfer on MHD three dimensional flow of Williamson fluid due to bidirectional non-linear stretching surface," *Results Phys.*, vol. 7, pp. 204–212, 2017, doi: 10.1016/j.rinp.2016.11.063.

[32] N. S. Khashi'ie, N. M. Arifin, I. Pop, R. Nazar, E. H. Hafidzuddin, and N. Wahi, "Three-Dimensional Hybrid Nanofluid Flow and Heat Transfer past a Permeable Stretching/Shrinking Sheet with Velocity Slip and Convective Condition," *Chinese J. Phys.*, vol. 66, no. July 2019, pp. 157–171, 2020, doi: 10.1016/j.cjph.2020.03.032.

[33] F. Sultan, W. A. Khan, M. Ali, M. Shahzad, M. Irfan, and M. Khan, "Theoretical aspects of thermophoresis and Brownian motion for three-dimensional flow of the cross fluid with activation energy," *Pramana - J. Phys.*, vol. 92, no. 2, pp. 1–10, 2019, doi: 10.1007/s12043-018-1676-0.

[34] T. Sajid, S. Tanveer, Z. Sabir, and J. L. G. Guirao, "Impact of Activation Energy and Temperature-Dependent Heat Source/Sink on Maxwell-Sutterby Fluid," *Math. Probl. Eng.*, vol. 2020, 2020, doi: 10.1155/2020/5251804.

[35] S. Vitanov, Dissertation-"Simulation of High Electron Mobility Transistors" *TU Wien Bibliothek.* pp. 48, December 2010.

[36] S. Krukowski *et al.*, "Thermal properties of indium nitride," *J. Phys. Chem. Solids*, vol. 59, no. 3, pp. 289–295, 1998, doi: 10.1016/S0022-3697(97)00222-9.

[37] P. Sreedevi and P. Sudarsana Reddy, "Effect of magnetic field and thermal radiation on natural convection in a square cavity filled with TiO2 nanoparticles using Tiwari-Das nanofluid model," *Alexandria Eng. J.*, vol. 61, no. 2, pp. 1529–1541, 2022, doi: 10.1016/j.aej.2021.06.055.

[38] S. Nandi and B. Kumbhakar, "Viscous Dissipation and Chemical Reaction Effects on Tangent Hyperbolic Nanofluid Flow Past a Stretching Wedge with Convective Heating and Navier's Slip Conditions," *Iran. J. Sci. Technol. - Trans. Mech. Eng.*, vol. 46, no. 2, pp. 379–397, 2021, doi: 10.1007/s40997-021-00437-1.

[39] T. V. Laxmi and B. Shankar, "Effect of Nonlinear Thermal Radiation on Boundary Layer Flow of Viscous Fluid over Nonlinear Stretching Sheet with Injection/Suction," *J. Appl. Math. Phys.*, vol. 04, no. 02, pp. 307–319, 2016, doi: 10.4236/jamp.2016.42038.

[40] T. Srinivasulu and B. S. Goud, "Effect of inclined magnetic field on flow, heat and mass transfer of Williamson nanofluid over a stretching sheet," *Case Stud. Therm. Eng.*, vol. 23, no. October 2020, p. 100819, 2021, doi: 10.1016/j.csite.2020.100819.

[41] B. Rushi, K. R. Sivaraj, and J. Prakash Editors, *Lecture Notes in Mechanical Engineering Advances in Fluid Dynamics*. 2018. [Online]. Available: http://www.springer.com/series/11693

[42] P. D. Ariel, "Generalized three-dimensional flow due to a stretching sheet," *ZAMM Zeitschrift fur Angew. Math. und Mech.*, vol. 83, no. 12, pp. 844–852, 2003, doi: 10.1002/zamm.200310052.

[43] H. A. Ogunseye, H. Mondal, P. Sibanda, and H. Mambili-Mamboundou, "Lie group analysis of a Powell–Eyring nanofluid flow over a stretching surface with variable properties," *SN Appl. Sci.*, vol. 2, no. 1, pp. 1–12, 2020, doi: 10.1007/s42452-019-1852-y.

[44] R. Kandasamy, R. Mohamad, and M. Ismoen, "Impact of chemical reaction on Cu, Al2O3 and SWCNTs–nanofluid flow under slip conditions," *Eng. Sci. Technol. an Int. J.*, vol. 19, no. 2, pp. 700–709, 2016, doi: 10.1016/j.jestch.2015.11.011.

[45] A. Hamid, Hashim, and M. Khan, "Impacts of binary chemical reaction with activation energy on unsteady flow of magneto-Williamson nanofluid," *J. Mol. Liq.*, vol. 262, pp. 435–442, 2018, doi: 10.1016/j.molliq.2018.04.095.

[46] T. Hayat, F. Shah, M. I. Khan, M. I. Khan, and A. Alsaedi, "Entropy analysis for comparative study of effective Prandtl number and without effective Prandtl number via γAl2O3-H2O and γAl2O3-C2H6O2 nanoparticles," *J. Mol. Liq.*, vol. 266, pp. 814–823, 2018, doi: 10.1016/j.molliq.2018.06.029.

[47] S. T. Hussain, S. Nadeem, and R. Ul Haq, "Model-based analysis of micropolar nanofluid flow over a stretching surface," *Eur. Phys. J. Plus*, vol. 129, no. 8, 2014, doi: 10.1140/epjp/i2014-14161-8.

Authors information:

First author:

Mamidala Jyotsna

Assistant professor of Mathematics,

Maturi Venkata Subba Rao (MVSR) Engineering college, (affiliated to Osmania University)

Nadergul, Hyderabad- 501510, India.

Second author:

Vadlakonda Dhanalaxmi

Professor of Mathematics,

University College of Technology,

Osmania University. Hyderabad- 500007, India.